Available online at www.sciencedirect.com
ScienceDirect
Carbohydrate Research 343 (2008) 512–520
Carbohydrate RESEARCH

Effects of cooling treatment and glutaraldehyde on the morphology of Au nanostructures synthesized from chitosan

Dongwei Wei, Weiping Qian,* Yi Shi, Shaohua Ding and Yan Xia

State Key Laboratory of Bioelectronics, Department of Biological Science and Medical Engineering, Southeast University, Nanjing 210096, PR China

Received 2 August 2007; received in revised form 25 October 2007; accepted 29 October 2007
Available online 5 November 2007

Abstract—A facile approach for the synthesis of chitosan-based Au nanostructures that have interesting absorptions in the near-infrared (NIR) region is presented. The effects of cooling treatment and the cross-linking agent glutaraldehyde on the formation of Au nanostructures based on chitosan were investigated. It has been demonstrated that the size and shape, and thus the optical properties of Au nanostructures, could be modulated via cooling treatment. The optical absorption extension of these Au nanostructures in the NIR region is promising in biomedical applications. The presence of a cross-linking agent, glutaraldehyde, during synthesis accelerated the reduction of the Au precursor and favored the growth of isotropic Au nanoparticles. A possible mechanism for the change in growth modality of Au nanostructures with and without glutaraldehyde was elucidated.
© 2007 Elsevier Ltd. All rights reserved.

Keywords: Nanostructures; Chitosan; Cooling treatment; Glutaraldehyde

1. Introduction

Metal nanoparticles have attracted intensive research interest because of their important applications in biomedicine, catalysis, and optics, as well as their use as antimicrobial agents and sensors.[1–8] As a result, many methods have been developed for the synthesis of metal nanoparticles in a wide range of nonspherical shapes, including wires, disks, cubes, prisms, hollow structures, dendrites, and tadpole nanocrystals.[9–14] Among these anisotropic nanostructures, two-dimensional (2D) nanoparticles with regular shapes (such as triangular), in particular, have captured considerable attention in recent years due to their attractive optical properties.[15–17] For example, Ag nanoplates display an in-plane dipole plasmon absorption peak that can be shifted to 1000 nm in the near-infrared (NIR) region.[18] Such an absorption extension opens possibilities in the biomedical and related fields.[18–21] In contrast to many protocols in the literature for the synthesis of 2D Ag nanostructures, relatively few reports are available for the preparation of such anisotropic Au nanostructures.[22–26]

It is known that polymers are often used to prepare metal nanoparticles in which the polar groups interact directly with the particle surface and strongly influence the shape of the particles.[23–27] Chitosan, a polysaccharide biopolymer derived from naturally occurring chitin, displays unique polycationic, chelating, and film-forming properties due to the presence of reactive amino and hydroxyl functional groups. With the development of chitosan science, chitosan and its many derivatives, which combine nontoxicity, biocompatibility, biodegradability, and bioactivity with attractive physical and chemical properties, are becoming increasingly important.[28,29] It has been documented that chitosan can be adopted as a stabilizer, and more recently, as a reducing agent to synthesize gold nanoparticles.[30–33] In the preliminary work,[34] we have recently demonstrated a facile method for the synthesis of 2D Au nanosheets on the basis of chitosan. This also was the first report on the preparation of such 2D Au nanostructures based on this technique. The nanosheets so produced exhibit a very broad in-plane plasmon band that extends well into

* Corresponding author. Tel./fax: +86 25 83795719; e-mail: wqian@seu.edu.cn

0008-6215/$ - see front matter © 2007 Elsevier Ltd. All rights reserved.
doi:10.1016/j.carres.2007.10.031

the NIR region. The NIR absorption of such gold nanostructures is promising for inducing hyperthermia in tumors and heat absorption in special equipment.[19–21] As is well known, glutaraldehyde was exploited as a conventional cross-linking agent to reinforce the chemical and mechanical properties of chitosan (film, bead, or hydrogel) and extend its application.[35–38] Given that chitosan has excellent film-forming characteristics, our study was based on preparing chitosan/glutaraldehyde/Au nanocomposite films by in situ self-assembly of the system containing tetrachloroauric acid, chitosan, and glutaraldehyde with the aim of developing substrates for biocatalysis. In this case, the investigation about the effect of glutaraldehyde on the formation of gold nanostructures in a chitosan system is desirable in that the microstructure of the preformed gold nanoparticles has an impact on their consequent interaction with bioactive enzymes immobilized on their surfaces. Interestingly, we found that the presence of glutaraldehyde during synthesis accelerated the reduction of the Au precursor and promoted the growth of isotropic nanoparticles. Thus, in the present paper, we present a further study on the synthesis of Au nanostructures by reduction of $AuCl_4^-$ ions with chitosan. The emphasis is on the investigation of the effects of cooling treatment and the cross-linking agent glutaraldehyde on the formation of gold nanostructures based on chitosan. We demonstrate that the modulation of the structural and optical properties of Au nanostructures could be realized via cooling treatment. The details of the investigation are presented below.

2. Experimental

2.1. Chemicals

Chitosan flakes from crab shells (Practical grade >85% deacetylated; Brookfield viscosity >200.000 cps) were of purchased from Aldrich Chemical Co. Hydrochloroauric acid, glutaraldehyde (25 wt %), and acetic acid were analytical grade. All compounds were used as received. Solutions were prepared with triply distilled water. Chitosan was dissolved in 1% acetic acid solution. Due to the poor solubility of chitosan, the mixture was kept overnight until a clear solution was obtained.

2.2. Synthesis

In a typical synthesis of Au nanostructures, 4 mL of 3–24 mM $HAuCl_4$, 6 mL of 3.46 mg/mL chitosan, and 1 mL of triply distilled water were mixed and stirred for homogenization. The mixture was transferred to a 12.5×2 cm cuvette and allowed to stand for about 6 h at the designated temperatures (between 40 and 100 °C), at the end of which time they were rinsed with triply distilled water and centrifuged to remove the residual reactants and possible contaminants and subjected to further characterization. Investigation of the cooling treatment on the formation of Au nanostructures was done by heating the parallel samples for a specified period of time at the same temperature and then leaving them at 4 °C for two weeks. Before characterization, the treatment procedures before analysis were the same as that for the products without cooling treatment. The effect of glutaraldehyde on the morphology of Au nanostructures was examined using procedures similar to those that were used for the preparation of Au nanostructures based on chitosan. The only difference was that 1 mL of deionized water was replaced with 1 mL of glutaraldehyde (5 wt %).

2.3. Characterization

Scanning electron microscopy (SEM) images were recorded by using an FEI SIRION field-emission scanning electron microscope equipped with energy-dispersive spectrum (EDS). Transmission electron microscopy (TEM) images were obtained by a JEM-2000EX microscope at an accelerating voltage of 120.0 kV. The optical properties of the as-prepared Au nanosheets were measured by a SHIMADZU UV–vis–NIR spectrophotometer (UV-3150).

3. Results and discussion

3.1. Characterization of Au nanosheets

Figure 1 shows a typical field-emission scanning electron microscopy (FESEM) image of the as-prepared samples. It is clear that Au nanosheets can be conveniently formed by reduction of $AuCl_4^-$ with chitosan. The product consists of an amount of micro-sized nanosheets that coexists with a few of the spherical particles as byproduct. Most nanosheets are triangular or hexagonal, approximately a few microns across. The product in Figure 1d is thin enough (approximately several tens of nanometers in thickness) that the electron beam can penetrate through a stack of overlaying sheets and allow the outlines of the underlying sheets to be seen.[39] The energy-dispersive spectrum (EDS) shows strong peaks assigned to elemental gold. Weak peaks for carbon and nitrogen are also present (Fig. 1e) and are attributed to the binding of polysaccharide residues to the particles.

Figure 2 presents a transmission electron microscopy (TEM) image for a single Au nanosheet (Fig. 2a), and the corresponding selected-area electron diffraction (SAED) pattern (Fig. 2b). The contrast within the truncated triangular nanosheet is mainly attributed to the existence of the internal stress, which comes from the deviations from the planar geometry (for some reasons,

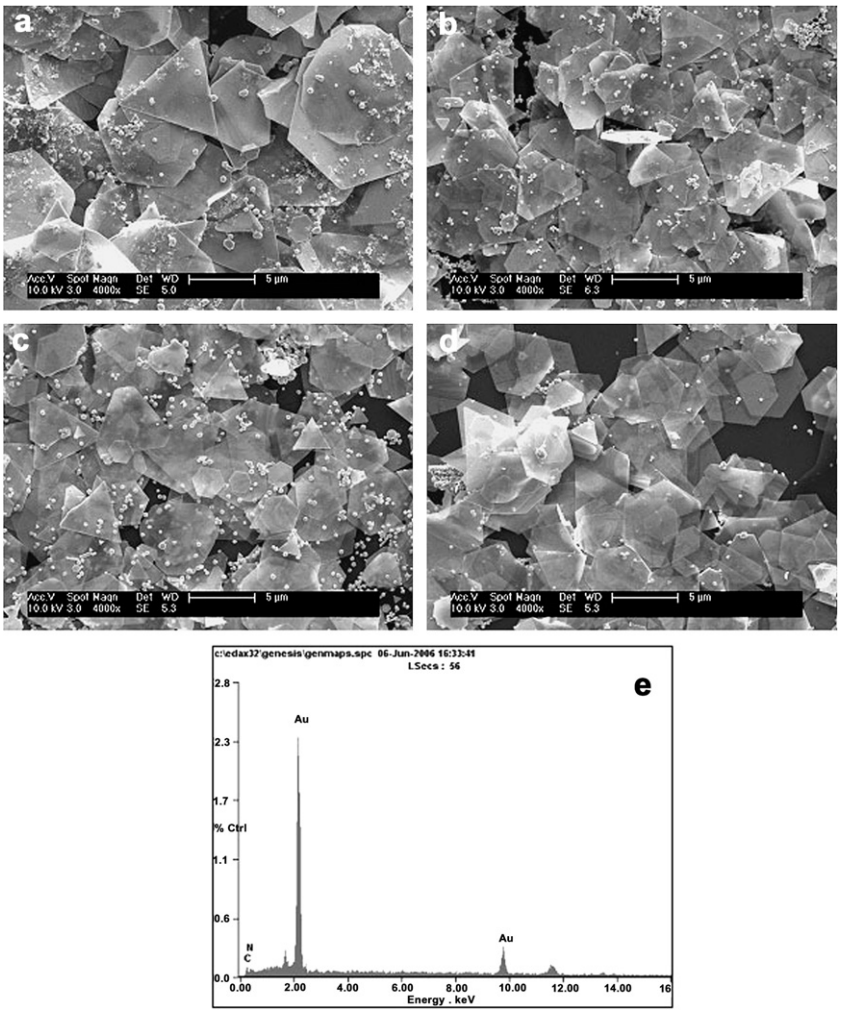

Figure 1. FESEM images of the sample synthesized by reduction of (a and c) 12 and (b and d) 8 of $HAuCl_4$ with chitosan (80 °C for a and b; 60 °C for c and d), (e) EDS of the Au nanosheets.

for example, stacking faults).[40,41] The SAED pattern viewed along a {1 1 1} direction is of hexagonal symmetry, indicating the single-crystal structure of the nanosheet.[23]

It is well known that the optical properties of metal nanostructures are strongly related to their shape and size.[21] For gold nanospheres, the absorption band at about 530 nm is assigned to the excitation of out-of-plane plasmon vibrations (also known as surface plasmon resonance or SPR) in the particles.[25] However, in the case of anisotropic nanostructures, more than one single resonance can be excited. The longer wavelength absorption band (>600 nm), attributed to in-plane plasmon vibrations, is a strong function of the aspect ratio and the physical dimensions of these nanostructures.[21,42] Under certain conditions of anisotropy, the in-plane plasmon band for these nanostructures can extend into the NIR region.[21,25,42] Figure 3 shows the optical absorption spectra of the Au nanosheets as formed dispersed in (a) water and (b) deposited on a glass substrate. It is apparent that, for the Au nanosheets dispersed in solution, the absorption spectrum displays an obvious increase in the band at ~500 nm, and then expands steadily into the near-IR region (Fig. 3a), which is in agreement with the results for Au sheet-like nanostructures reported previously.[25,26] The spectra recorded from the glass substrate (Fig. 3b) also exhibit such significant absorption in the near-IR region. This broad and asymmetric band may be arising from the higher order resonances of Au nanostructures.[25,42] Such an absorption extension of these Au nanosheets in the near-IR region may be useful in biomedical applications.[19–21,23] The peak at ~850 nm, which also appears in the optical spectra below, should be attributed to instrument noise originating from the light source.

3.2. Effect of cooling treatment on the morphology of Au nanostructures

Figure 4 compares the optical spectra of the Au nanostructures synthesized from chitosan with (curve 2) and without (curve 1) cooling treatment. Three obvious

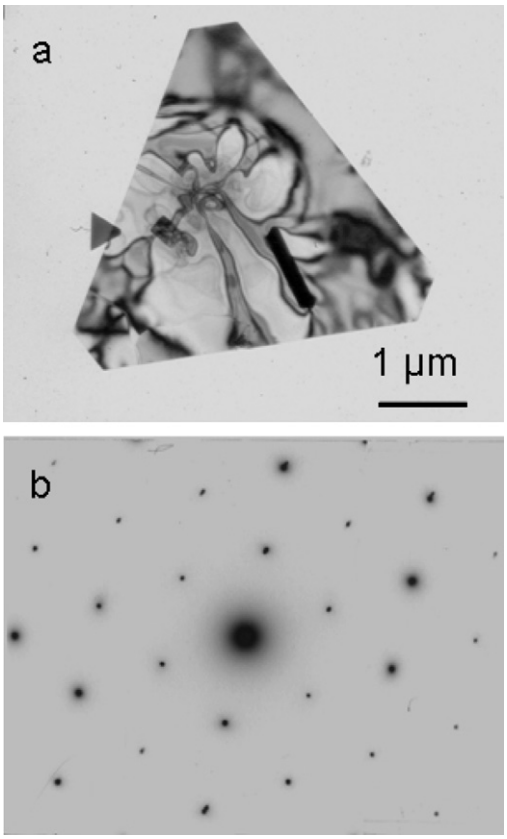

Figure 2. (a) TEM image of a single Au nanosheet. (b) The corresponding SAED pattern.

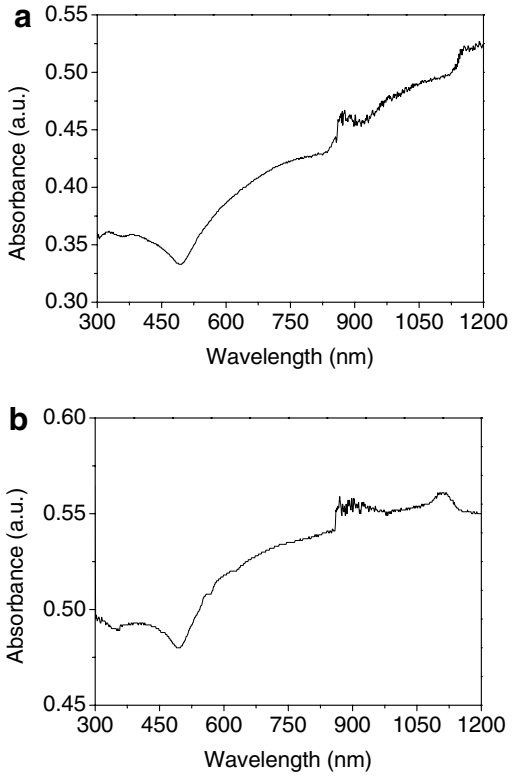

Figure 3. The optical absorption spectra of the sample synthesized by reduction of 12 mM $HAuCl_4$ utilizing chitosan at 80 °C. (a) Dispersed in water and (b) deposited on a glass substrate.

features are observed from these spectra. Firstly, it is clear from curve 1, Figure 4a, that there are two absorption bands (the band <400 nm is not discussed here): one is within the 500–600 nm region and the other is at 600–900 nm. The absorption band in the 500–600 nm region is assigned to the dipole resonance associated with spherical Au nanoparticles.[21] The other one (600–800 nm) mainly arises from the strong interparticle interaction among aggregates or the deviation from spherical geometry of gold nanoparticles.[31] However, the absorption spectrum of the Au product with cooling crystallization (curve 2) displays an obvious absorption extension into the near-IR region, which is consistent with the spectrum of the above-mentioned anisotropic Au nanosheets (Fig. 3). Secondly, it is observed that, with and without cooling treatment, the optical spectrum of Au products shows obvious distinction, even though they both exhibit anisotropic characteristics (compare curve 1 with cuve 2 in Fig. 4b and c, respectively). These may suggest that the Au nanostructures have a distinctness in morphology since the longer wavelength absorption band is sensitive to the physical dimensions of Au products such as edge length, sharpness, and thickness.[42] Thirdly, an observation is that, with cooling treatment, the optical spectrum of the samples undergoes a switch from one absorption band at ~560 nm (curve 1 in Fig. 4d) to two absorption bands at ~560 nm and at 600–900 nm, respectively (curve 2 in Fig. 4d), which indicates the formation of either anisotropic or aggregated Au nanoparticles.[31]

Further evidence for cooling treatment dependent variation in Au morphology is provided by TEM analysis (Fig. 5). Three important observations are made from these images. The first is that a switching of the morphology of the Au nanostructures from spherical nanoparticles about 100 nm in size, together with a few small gold nanosheets (without cooling treatment, Fig. 5A), to micro-sized nanosheets with regular shape (with cooling treatment, Fig. 5a) was observed, as evidenced by the results of the optical absorption spectra in Figure 4a. The second is that the sizes of nanosheets with cooling are obviously smaller than those without cooling (compare Fig. 5b and B, c and C), indicating that cooling treatment induces the variability of the physical dimensions of Au nanosheets,[42] which accounts for the dissimilar spectral signatures in the comparison of curve 1 with curve 2 in Figure 4b and c, respectively. The last observation is that the anisotropic Au nanostructures are present after cooling treatment (Fig. 5d), which is consistent with the obvious anisotropic characteristics in the plasmon resonance spectrum in Figure 4d. Therefore, the size and shape,

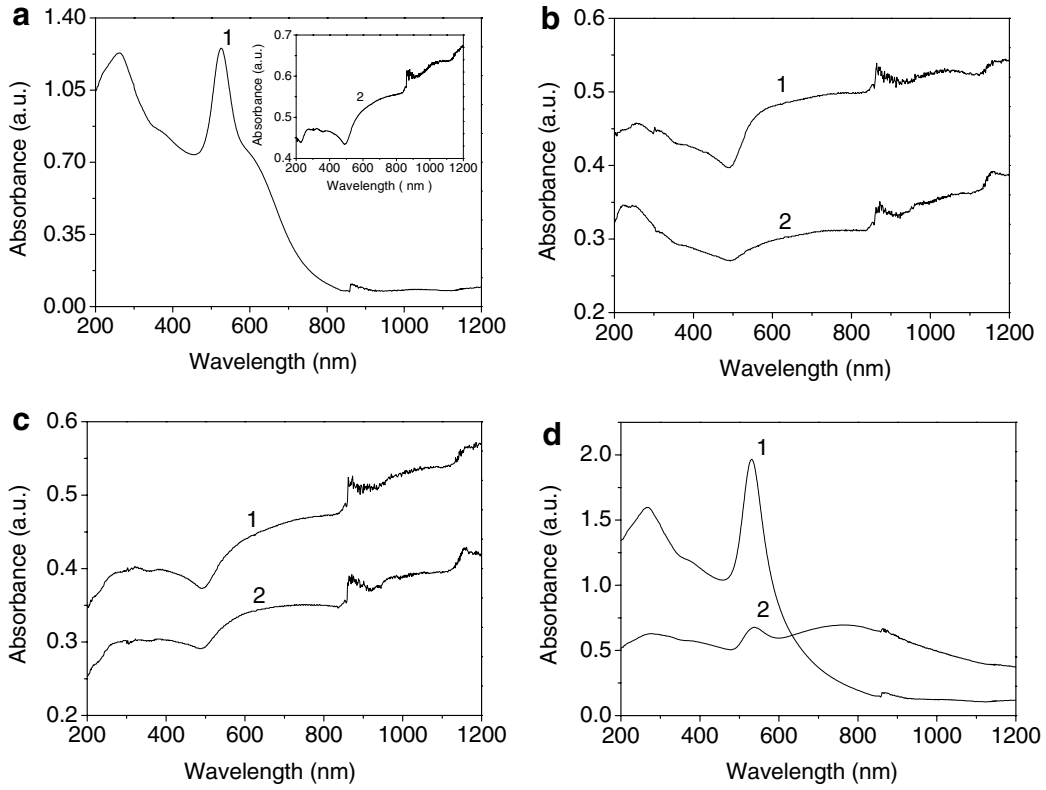

Figure 4. Optical absorption spectra of the samples synthesized by reduction of $HAuCl_4$ utilizing chitosan with (2) and without (1) cooling treatment. (a): 100 °C for (1) 6 h and for (2) 80 min; (b): 80 °C for (1) 6 h and for (2) 80 min; (c): 60 °C for (1) 6 h and for (2) 120 min; (d): 60 °C for (1) 6 h and for (2) 120 min. Concentration of $HAuCl_4$: 24 mM for b; 12 mM for a; 8 mM for c; 3 mM for d. The resulting products from (1) were rinsed and centrifuged for further characterization soon after the reaction was over, and the products from (2) were left at 4 °C for two weeks before analysis. For further details refer to Section 2.

and hence the optical properties of Au nanostructures, can be manipulated by the cooling treatment.

As demonstrated in our recent work,[34] Au monomers are produced by reducing $AuCl_4^-$ ions with chitosan molecules and/or some molecules induced by reaction. When the concentration of gold atoms has reached supersaturation, a system that is far from the minimum free-energy configuration, they start to nucleate and grow. Then at a favorite chitosan coverage, the preferential adsorption of polar groups (such as hydroxyl and/or amino groups) in chitosan molecules on the {1 1 1} planes of the Au nucleus may account for the formation of anisotropic nanosheets.

It has been discussed by Xia and co-workers[43] that the reduction temperature has an impact on both the shape and size of the metal nanostructures. On one hand, slow reduction at low temperatures greatly reduced the level of supersaturation and thus the quantity of seeds formed in the nucleation step. At the same concentration of metal precursor, a decrease in the quantity of the number of seeds resulted in the formation of larger-sized nanoparticles. On the other hand, the reduction rate, depending on the temperature, was critical to the control of reduction kinetics and hence the formation of anisotropic nanosheets. As the temperature was decreased, the yield of nanosheets decidedly increased. We surmise that these two principles should be accountable for our results that, in comparison with the products shown in Figure 5A and a, D and d, the nanostructures prepared with cooling treatment were much bigger and that the ratio of anisotropic nanosheets was increased.

Moreover, after heating for 80 or 120 min at z designated temperature, there exist Au^0 atoms and Au clusters in the solution in addition to the Au nanosheets formed during thermal treatment.[44] During the subsequent cooling crystallization, the Au nanosheets formed will serve as 'seeds' and grow by attachment of the residual Au^0 atoms and Au clusters via the Ostwald ripening process[22] along the ⟨1 1 1⟩ direction due to high surface energy and weak adsorption of chitosan on the {1 1 0} planes, leading to the increase of the planar dimension. After exhaustion of the remaining Au^0 atoms and Au clusters in the solution, the size of the Au nanosheets will not be increased. However, the nanosheets without cooling can continuously grow by attachment of the Au^0 atoms produced under thermal treatment until $AuCl_4^-$ reduction is completed. This may explain the formation of smaller sized anisotropic Au nanosheets after cooling treatment (compare Fig. 5b with B, c with C).

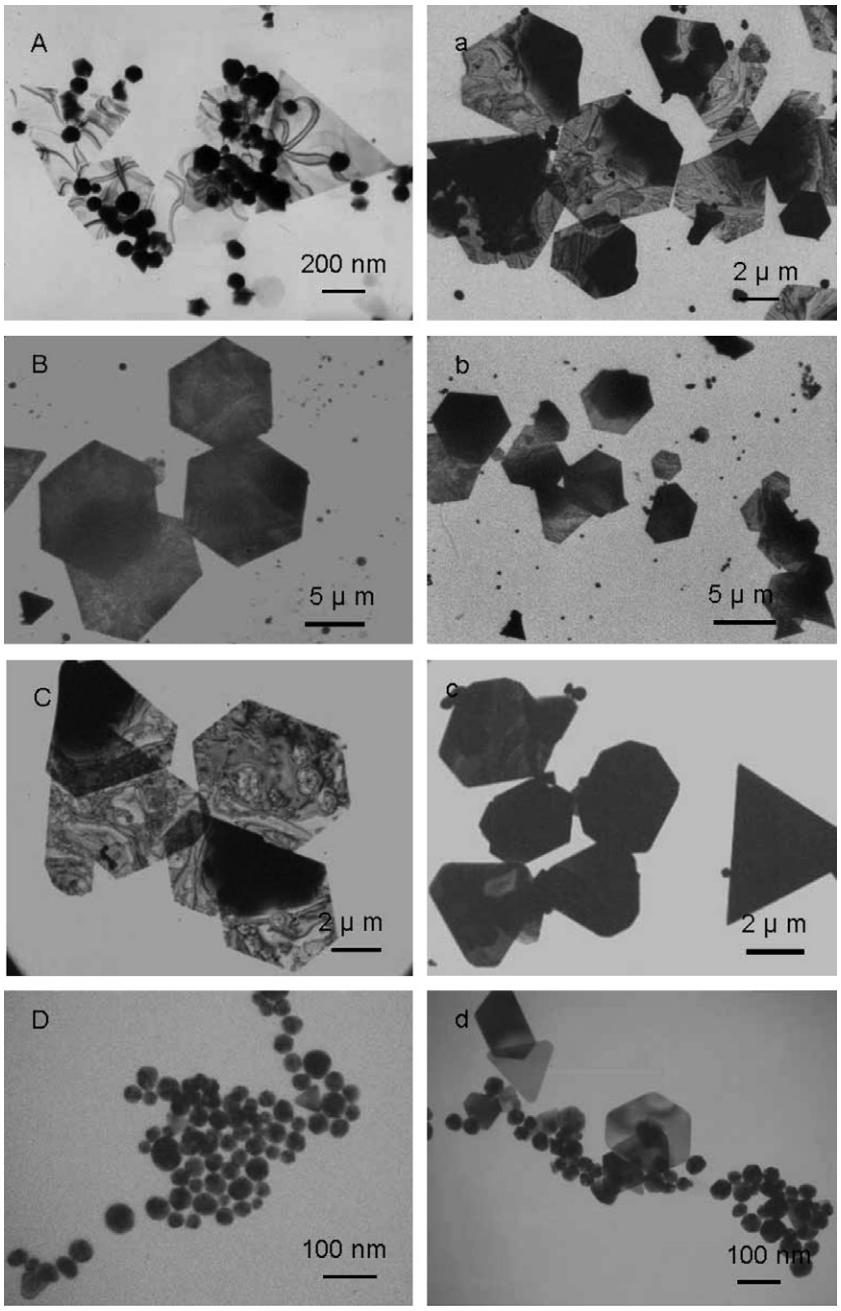

Figure 5. TEM images for Au nanostructures with (a, b, c, and d) and without (A, B, C, and D) cooling treatment: (A) 100 °C for 6 h and (a) for 80 min; (B) 80 °C for 6 h and (b) for 80 min; (C) 60 °C for 6 h and (c) for 120 min; (D) 60 °C for 6 h and (d) for 120 min. Concentration of $HAuCl_4$: 24 mM for B, b; 12 mM for A, a; 8 mM for C, c; 3 mM for D, d. The resulting products from (A, B, C, and D) were rinsed and centrifuged for further characterization soon after the reaction was over, and the products from (a, b, c, and d) were left at 4 °C for two weeks before analysis. For further details refer to Section 2.

3.3. Effect of glutaraldehyde on the morphology of Au nanostructures

A series of experiments have been carried out to study the effect of glutaraldehyde, a typical cross-linking agent of chitosan, on the synthesis of nanostructures based on chitosan. The optical spectra of the Au products as-prepared in the presence (curve 1) and absence (curve 2) of glutaraldehyde are shown in Figure 6. It is clear that the samples prepared in the presence of glutaraldehyde show the characteristic SPR band of gold nanoparticles centered at ~530 nm.[25] The samples produced in the absence of glutaraldehyde, nevertheless, show an obvious absorption extension in the near-IR region characteristic feature of the above-mentioned anisotropic Au nanosheets.[23,25]

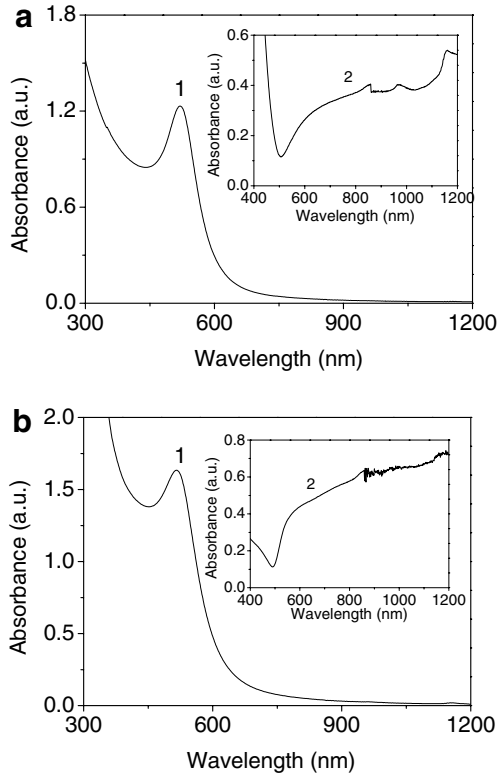

Figure 6. The optical absorption spectra of the sample synthesized (1) with and (2) without glutaraldehyde. (a) 12 mM $HAuCl_4$, 60 °C; (b) 8 mM $HAuCl_4$, 80 °C.

Typical TEM images of Au nanostructures (a) with and (b) without glutaraldehyde by reduction of $AuCl_4^-$ ions with chitosan are shown in Figure 7. It is observed that the presence of glutaraldehyde promotes the generation of isotropic gold nanoparticles (Fig. 7a), which provide evidence for the UV–vis measurement (Fig. 6a). On the other hand, the product synthesized in the absence of glutaraldehyde was mainly composed of micro-sized anisotropic nanosheets (Fig. 7b), which is consistent with the FESEM characterization shown in Figure 1c.

In another experiment, we found that, when glutaraldehyde is absent, no absorption peak was observed in a system with 4 mL of 1 mM $HAuCl_4$ and 6 mL of 3.46 mg/mL chitosan at 60 °C for 30 min (Fig. 8a); however, the absorption value of the sample shows a drastic increase upon the addition of a small amount of glutaraldehyde (Fig. 8b).

The exact role of glutaraldehyde on the formation of Au nanostructures during synthesis was studied in detail by altering its concentration, as shown in Figure 9. As we know, changes in absorbance cannot be directly related to the kinetic change in concentration of the formed nanoparticles as its size changes during the reaction and produces a variation in the extinction coefficient.[45] Nevertheless, such changes allow comparing the roughly kinetic behavior of reactions in which no important differences in final shape and size are observed and have been frequently used to evaluate nanoparticles formation.[45,46] It is clear from Figure 9 that the optical absorption values of gold nanostructures increase with the increasing amount of glutaraldehyde, indicating the increased formation rate of Au nanoparticles.

In a supplemental experiment, we found that the yield of nanoparticles was very close to zero when chitosan was absent in the solution after 12 h at 25 °C; nevertheless, an elevated temperature does produce nanoparticles. The reason may be that glutaraldehyde, as a weak reducing agent, could not directly induce the formation of gold 'seed' and thus the nanoparticles at relatively low temperature. It is also worth noting that, in all experiments, a clear chitosan solution was obtained other than precipitation or chitosan hydrogels, which should be due to the content of glutaraldehyde added being far less than that of the chitosan in the system. Meantime, we found that the sequence of the addition of glutaraldehyde has little influence on the reduction of the Au precursor.

In summary, the introduction of glutaraldehyde accelerated the reduction of the Au precursor and consequently switched sheet-like growth of gold to sphere-

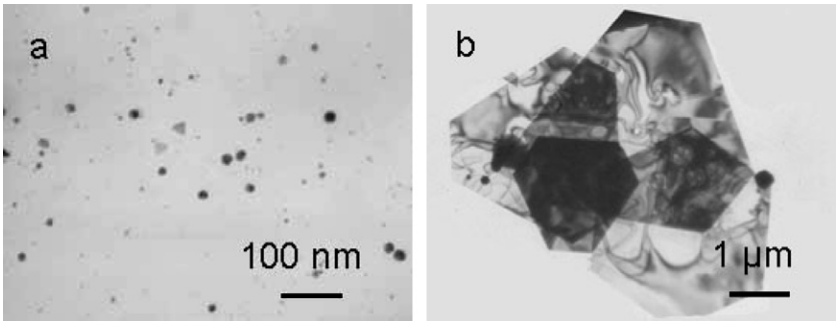

Figure 7. Representative TEM images of Au products synthesized (a) with and (b) without glutaraldehyde in a chitosan solution (12 mM $HAuCl_4$, 60 °C).

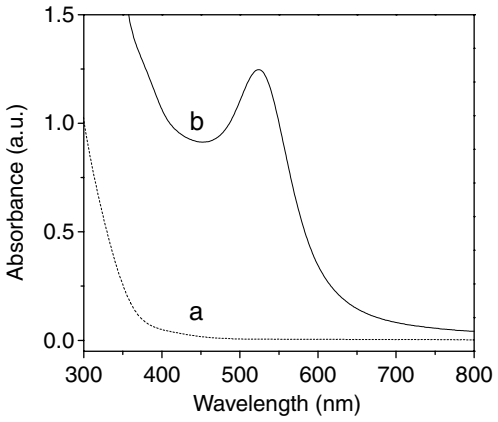

Figure 8. The optical absorption spectra of the Au products synthesized by reduction of 1 mM $HAuCl_4$ with chitosan in the (a) absence and (b) presence of 4.5×10^{-2} M glutaraldehyde at 60 °C for 30 min.

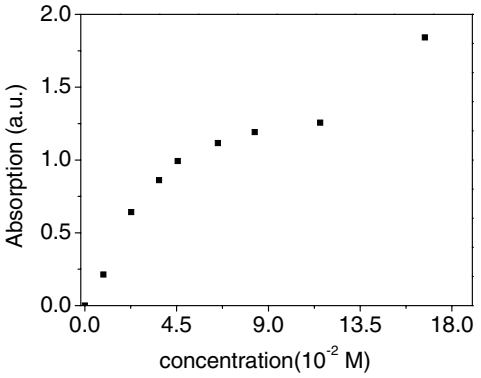

Figure 9. The change of optical absorption values of gold nanostructures (523 nm) as a function of glutaraldehyde concentrations synthesized in a system with $HAuCl_4$ (4 mL, 1 mM) and chitosan (6 mL, 3.46 mg/mL) at 25 °C for 30 min.

like particles. Although it is not clear how glutaraldehyde molecules impact the reduction of the Au precursor in chitosan solution, we suggest that two possible factors could explain the above results. Firstly, the weakly reductive activity of glutaraldehyde may promote the fast reduction of the Au precursor. Secondly, the presence of glutaraldehyde partly destroys the hydrogen bonding between the interior molecules or chitosan chains and improves the hydrophilicity of chitosan by the release of some controlled amino and hydroxyl groups in its chains (we did observe that the viscosity of the reaction solution decreased after glutaraldehyde was introduced). Consequently, the reductive sites in chitosan molecules are more easily accessible to $AuCl_4^-$ ions, which also contribute to the fast formation of Au particles. Due to the concentration of Au atoms induced by chitosan and/or some molecules produced by the reaction being far below supersaturation, no nucleation and growth had taken place in the system without glutaraldehyde even when reacted at 60 °C for 30 min (Fig. 8a).[47] The presence of a small amount of glutaraldehyde accelerated the formation of Au nuclei and greatly increased the level of supersaturation, and hence the number of seeds formed in the nucleation step. At the same concentration of Au precursor, an increase in the number of seeds resulted in the formation of isotropic Au nanoparticles (curve 1 in Fig. 6a and b).[43,47] Whether Au atoms are catalyzed by preformed nanoparticles in the solution during the particle formation is not known.[45]

4. Conclusions

The synthesis of Au nanostructures with interesting absorption in the NIR region has been carried out by the reduction of $AuCl_4^-$ ions with chitosan. We demonstrated that it was possible to modulate the size and shape, and hence the optical properties of Au nanostructures by a cooling treatment. The tunable absorption in the NIR region of such nanostructures may be useful in the biomedical or related fields. The presence of glutaraldehyde during synthesis accelerated the reduction of the Au precursor and favored the growth of isotropic Au nanoparticles. This facile approach for preparing Au nanostructures under such typical conditions may be extended to prepare chitosan/glutaraldehyde/Au nanocomposite films, beads, or hydrogels aiming at biomedical or related applications (the participation of glutaraldehyde is alternative).

Acknowledgments

This research is supported by the Foundation for the Author of National Excellent Doctoral Dissertation of PR China (No. 200252), and the Foundation for Excellent Doctoral Dissertation of Southeast University.

References

1. Wang, X.; Zhuang, J.; Peng, Q.; Li, Y. D. *Nature* **2005**, *437*, 121–124.
2. Rameshbabu, N.; Sampath Kumar, T. S.; Prabhakar, T. G.; Sastry, V. S.; Murty, K. V. G. K.; Rao, K. P. *J. Biomed. Mater. Res. A* **2007**, *80*, 581–591.
3. Porel, S.; Singh, S.; Harsha, S. S.; Rao, D. N.; Radhakrishnan, T. P. *Chem. Mater.* **2005**, *17*, 9–12.
4. Ding, S. H.; Qian, W. P.; Tan, Y.; Wang, Y. *Langmuir* **2006**, *22*, 7105–7108.
5. Singh, A.; Hede, S.; Sastry, M. *Small* **2007**, *3*, 466–473.
6. Tan, Y.; Qian, W. P.; Ding, S. H.; Wang, Y. *Chem. Mater.* **2006**, *18*, 3385–3389.
7. Sun, J. M.; Ma, D.; Zhang, H.; Liu, X. M.; Han, X. W.; Bao, X. H.; Weinberg, G.; Pfänder, N.; Su, D. S. *J. Am. Chem. Soc.* **2006**, *128*, 15756–15764.

8. You, C. C.; Agasti, S. S.; De, M.; Knapp, M. J.; Rotello, V. M. *J. Am. Chem. Soc.* **2006**, *128*, 14612–14618.
9. Wiley, B.; Sun, Y. G.; Mayers, B.; Xia, Y. N. *Chem. Eur. J.* **2005**, *11*, 454–463.
10. Sau, T. K.; Murphy, C. J. *J. Am. Chem. Soc.* **2004**, *126*, 8648–8649.
11. Murphy, C. J.; Sau, T. K.; Gole, A. M.; Orendorff, C. J.; Gao, J. X.; Gou, L. F.; Hunyadi, S. E.; Li, T. *J. Phys. Chem. B* **2005**, *109*, 13857–13870.
12. Chen, Y. B.; Chen, L.; Wu, L. M. *Inorg. Chem.* **2005**, *44*, 9817–9822.
13. Wiley, B. J.; Xiong, Y. J.; Li, Z. Y.; Yin, Y. D.; Xia, Y. N. *Nano Lett.* **2006**, *6*, 765–768.
14. Lou, X. W.; Yuan, C. L.; Archer, L. A. *Chem. Mater.* **2006**, *18*, 3921–3923.
15. Shankar, S. S.; Rai, A.; Ankamwar, B.; Singh, A.; Ahmad, A.; Sastry, M. *Nat. Mater.* **2004**, *3*, 482–488.
16. Ankamwar, B.; Chaudhary, M.; Sastry, M. *Synth. React. Inorg., Met.-Org. Nano-Met. Chem.* **2005**, *35*, 19–26.
17. Dahanayaka, D. H.; Wang, J. X.; Hossain, S.; Bumm, L. A. *J. Am. Chem. Soc.* **2006**, *128*, 6052–6053.
18. Chen, S. H.; Carroll, D. L. *J. Phys. Chem. B* **2004**, *108*, 5500–5506.
19. Hirsch, L. R.; Stafford, R. J.; Bankson, J. A.; Sershen, S. R.; Rivera, B.; Price, R. E.; Hazle, J. D.; Halas, N. J.; West, J. L. *Proc. Natl. Acad. Sci. U.S.A.* **2003**, *100*, 13549–13554.
20. Sershen, S. R.; Westcott, S. L.; Halas, N. J.; West, J. L. *J. Biomed. Mater. Res.* **2000**, *51*, 293–298.
21. Shankar, S. S.; Rai, A.; Ahmad, A.; Sastry, M. *Chem. Mater.* **2005**, *17*, 566–572.
22. Wiley, B.; Sun, Y. G.; Chen, J. Y.; Cang, H.; Li, Z. Y.; Li, X. D.; Xia, Y. N. *MRS Bull.* **2005**, *30*, 356–361.
23. Li, C. C.; Cai, W. P.; Cao, B. Q.; Sun, F. Q.; Li, Y.; Kan, C. X.; Zhang, L. D. *Adv. Funct. Mater.* **2006**, *16*, 83–90.
24. Sun, X. P.; Dong, S. J.; Wang, E. K. *Langmuir* **2005**, *21*, 4710–4712.
25. Kan, C. X.; Zhu, X. G.; Wang, G. H. *J. Phys. Chem. B* **2006**, *110*, 4651–4656.
26. Sun, X. P.; Dong, S. J.; Wang, E. K. *Angew. Chem., Int. Ed.* **2004**, *43*, 6360–6363.
27. Wei, D. W.; Qian, W. P. *J. Nanosci. Nanotechnol.* **2006**, *6*, 2508–2514.
28. Yi, H.; Wu, L. Q.; Bentley, W. E.; Ghodssi, R.; Rubloff, G. W.; Culver, J. N.; Payne, G. F. *Biomacromolecules* **2005**, *6*, 2881–2894.
29. Lin, Y. W.; Chen, Q.; Luo, H. B. *Carbohydr. Res.* **2007**, *342*, 87–95.
30. Esumi, K.; Takei, N.; Yoshimura, T. *Colloids Surf., B* **2003**, *32*, 117–123.
31. Huang, H. Z.; Yang, X. R. *Biomacromolecules* **2004**, *5*, 2340–2346.
32. Dos Santos, D. S.; Goulet, P. J. G.; Pieczonka, N. P. W.; Oliverira, O. N.; Aroca, R. F. *Langmuir* **2004**, *20*, 10273–10277.
33. Wang, B.; Chen, K.; Jiang, S.; Reincke, F.; Tong, W.; Wang, D.; Gao, C. Y. *Biomacromolecules* **2006**, *7*, 1203–1209.
34. Wei, D. W.; Qian, W. P.; Shi, Y.; Ding, S. H.; Xia, Y. *Carbohydr. Res.* **2007**, *342*, 2494–2499.
35. Webster, A.; Halling, M. D.; Grant, D. M. *Carbohydr. Res.* **2007**, *342*, 1189–1201.
36. Crescenzi, V.; Francescangeli, A.; Taglienti, A.; Capitani, D.; Mannina, L. *Biomacromolecules* **2003**, *4*, 1045–1054.
37. Berger, J.; Reist, M.; Mayer, J. M.; R Gurny, O. F. *Eur. J. Pharm. Biopharm.* **2004**, *57*, 35–52.
38. Ye, P.; Xu, Z. K.; Wu, J.; Innocentd, C.; Seta, P. *Biomaterials* **2006**, *27*, 4169–4176.
39. Chu, H. C.; Kuo, C. H.; Huang, M. H. *Inorg. Chem.* **2006**, *45*, 808–813.
40. Ding, Y.; Wang, Z. L. *J. Phys. Chem. B* **2004**, *108*, 12280–12291.
41. Rodríguez-González, B.; Pastoriza-Santos, I.; Liz-Marzán, L. M. *J. Phys. Chem. B* **2006**, *110*, 11796–11799.
42. Millstone, J. E.; Park, S.; Shuford, K. L.; Qin, L.; Schatz, G. C.; Mirkin, C. A. *J. Am. Chem. Soc.* **2005**, *127*, 5312–5313.
43. Xiong, Y. J.; McLellan, J. M.; Chen, J. Y.; Yin, Y. D.; Li, Z. Y.; Xia, Y. N. *J Am. Chem. Soc.* **2005**, *127*, 17118–17127.
44. Li, C. C.; Cai, W. P.; Li, Y.; Hu, J. L.; Liu, P. S. *J. Phys. Chem. B* **2006**, *110*, 1546–1552.
45. Eustis, S.; Hsu, H. Y.; El-Saved, M. A. *J. Phys. Chem. B* **2005**, *109*, 4811–4815.
46. Hoppe, C. E.; Lazzari, M.; Pardiñas-Blanco, I.; López-Quintela, M. A. *Langmuir* **2006**, *22*, 7027–7034.
47. Burda, C.; Chen, X. B.; Narayanan, R.; El-Sayed, M. A. *Chem. Rev.* **2005**, *105*, 1025–1102.